Steady-State Multiplicity, Flashback, and Control Issues in CH_4 Radiant Burners

M. Bizzi, G. Saracco, and V. Specchia
Dept. of Materials Science and Chemical Engineering, Politecnico di Torino, C.so Duca degli Abruzzi 24, 10129 Torino (TO), Italy

DOI 10.1002/aic.10183
Published online in Wiley InterScience (www.interscience.wiley.com).

Methane is widely employed as a source of energy in combustion systems. Among the currently available technologies, radiant heaters offer high thermal efficiency and low environmental impact in comparison with atmospheric burners. The present work deals with the modeling of methane combustion in a noncatalytic metal fiber burner, represented by means of one-dimensional transient equations. The model accounts for a detailed reaction mechanism, radiation within the porous medium, longitudinal heat and mass transfer. After its validation, the model was employed to analyze a typical stability problem that affects these systems: under given operating conditions (low specific power inputs and excess of air) the occurrence of flashback may in fact preclude the safe operation of the system. As a consequence of energy radiation in the upstream direction, the burner upstream surface and the plenum chamber might become hot enough to heat in turn the gas feedstock, thus eventually determining flashback. In this paper, the mechanism of flashback is numerically investigated as a function of the burner structure and operating conditions by means of a model analysis so as to single out regions of flashback occurrence and a criterion for safe operation. Finally, some guidelines are outlined for a cheap and effective control of the system, paving the way for possible improvement of currently adopted control systems. © 2004 American Institute of Chemical Engineers *AIChE J,* 50: 2276–2286, 2004

Keywords: natural gas combustion; modeling; reaction engineering; metal fibre burners; flashback; process control

Introduction

In the past decades, the growing importance of methane as a power source considerably increased the efforts devoted to the development of efficient and safe combustion systems. In this context, radiant premixed burners offer superior performance compared to traditional diffusive-type ones in terms of thermal efficiency, environmental impact, and design flexibility (Hargreaves et al., 1986; Saracco et al., 1999). Due to the considerable heat exchange between the reacting gas and the porous medium and the radiative output of the latter, lower flame temperatures can be achieved, thus allowing a remarkable reduction of NO_x emissions. The design of these devices may be approached by making more compact geometries of the combustion chamber and of the heat exchanger. Furthermore, burners can be operated firing upward, downward, or sideways, as opposite to diffusive-type burners. Moreover, the system can be operated at lower excess of air, thus promoting high flue gas temperatures. This improves, in turn, the performance of the heat exchanger, due to the increment in the driving force of the heat transfer process, resulting in enhanced thermal efficiency.

However, these devices might suffer from serious flame stability problems typically associated with the occurrence of flashback phenomena, which take place as a result of the gas feedstock preheating. Once the flame front is stabilized within the porous medium, the upstream surface of the fiber mat reaches relatively high temperatures. Radiation of energy in the upstream direction determines a broad increase of the burner

Correspondence concerning this article should be addressed to G. Saracco at guido.saracco@polito.it.

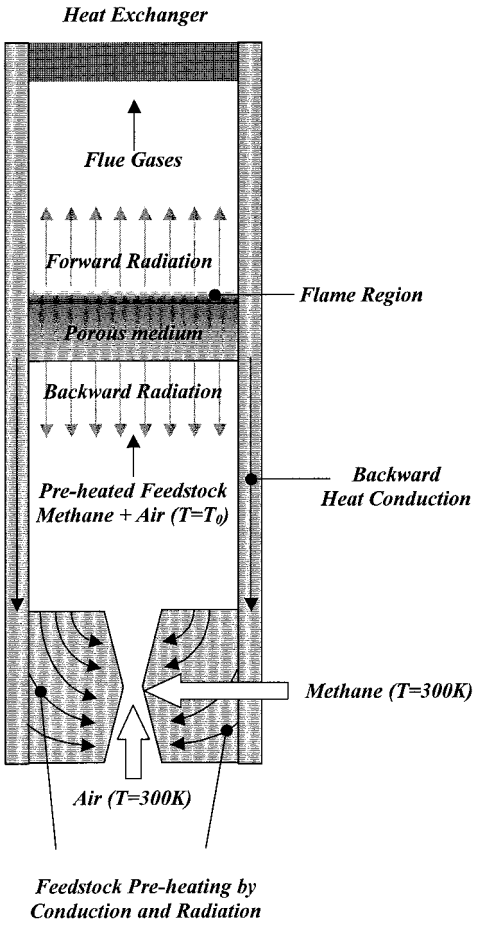

Figure 1. Premixed burner setup.

housing temperature which entails, in turn, a preheating of the gas stream entering the combustion system (Figure 1). Therefore, the flame front moves upstream within the porous medium, as a result of the increased inlet gas temperature that enhances chemical reactivity. This determines a further increase in the upstream surface temperature and in the upstream energy flux by radiation, eventually promoting the reactant's ignition ahead of the porous medium (flashback occurrence).

In order to enhance system performance and safety, improved understanding of the principles governing radiant premixed burners has become imperative and extensive modeling activities were carried out for this purpose (Rumminger, 1996; Bouma, 1997). In this article, an analysis of the stability of a noncatalytic metal fiber burner is presented, with particular attention to the occurrence of flashback. The burner model is coupled with an energy balance for the preheating of the feedstock that allows one to predict the potential of flashback occurrence. By means of the present analysis, a range of operating conditions can be singled out where safe operation can be achieved and some indications on optimal control strategies derived.

The analysis presented in this work can be divided into three parts:

Model validation and burner thermal behavior: in the first part of the work the burner model is validated against a set of experimental data. The comparison was carried out on the burner surface temperatures (upstream and downstream) at different values of excess of air and specific power input. This analysis allows the observation that the model reproduces the thermal behavior of the system, which is investigated in detail, being a critical aspect for the understanding of flashback. Finally, for the sake of completeness, a comparison in terms of CO and CO_2 emissions is also proposed;

Flashback analysis: in the second part of the work, the model was used to understand the physics of flashback occurrence. An analysis is performed on the "mechanism" generating flashback and on steady-state multiplicity. A final comparison between calculation and experimental data on flashback is also proposed;

Flashback avoidance and control issues: the last part of the activity focuses on the development of an improved anti-flashback control strategy to be implemented on commercial units.

Experimental Procedures

A pilot plant of the maximum power of 40 kW was employed to produce the experimental data used as the target of the numerical analysis. The adopted boiler configuration and the related experimental procedure were extensively described by Cerri et al. (2001); some details are nonetheless here provided. The feed gas streams, air and methane, are premixed in a Venturi, with the air mass flow rate determined by a blower and the methane flow rate by a modulating electrovalve. The burner operating conditions are generally parameterized in terms of specific power input Q and excess of air E_a. The former represents the energy input of the burner per unit surface area of porous medium and is proportional to the methane flow rate. The latter represents the excess of air used in the combustion referred to the stoichiometric requirement; the value of this parameter is therefore 0% if the combustion is carried out using a stiochiometric mixture of CH_4 and air. The thermal load required by the user controls the blower speed, whereas the opening of the electrovalve is driven by the pressure drop of the gas feedstock throughout the Venturi. As the air flow rate increases, the gas velocity and the pressure drop rise, and this signal is used to increase the methane flow rate. By proper screw regulation of the electrovalve sensitivity to pressure variation, sets of variable Q values under quasi-stationary E_a conditions can be obtained. In the plenum chamber, the distribution of the gas over the porous medium is accomplished by a system of perforated plates, in order to obtain a uniform flow field. The porous medium (a FeCrAlloy NIT100S fiber mat) is placed horizontally, at the end of the plenum chamber, and is firing upward. The external walls of the combustion chamber are provided with windows for observing the burner surface under operation. Just above the combustion chamber, the flue gases were cooled through a "finned-tube"-type heat exchanger and dispersed through a chimney after gas sampling for composition analysis. The composition of the exhaust gas was monitored by means of a set of continuous Elsag–Bailey analyzers: a NO_x chemiluminescence analyzer, a ND analyzer for CO and CO_2, and an O_2 paramagnetic detector. The surface temperatures of the upstream and downstream burner surfaces were recorded for each test through specific thermocouples placed on the metal fiber mat.

Test runs were carried out in the range of specific power

inputs from 200 to 800 kW/m^2 at different excess of air values (from to 5 to 90%). The experimental data were obtained by systematic runs of the pilot plant so as to span a wide range of operating conditions ranging from radiant heat regime (the burner is radiating as a significant fraction of methane combustion takes place within its thickness) to blue flame mode (a carpet of blue flames is formed downstream of the burner). Measured values of temperatures and compositions were reported at each Q and E_a value, and the results can be found in the article by Cerri et al. (2001). In particular, the temperature measurements were corrected in order to account for radiation, occurring at the thermocouple tip, according to a criterion suggested in the literature (Xiao et al., 2000).

For the investigation of the burner stability, Q was modulated stepwise ($\Delta Q \geq 20$ kW/m^2) from a stable radiant regime ($Q = 500$ kw/m^2) down to occurrence of flashback at selected values of E_a. To investigate flashback, a longer run was carried out on the burner. At the operating conditions (Q, E_a) under investigation, flashback occurrence was excluded when stable burner operation was continuously guaranteed for at least 15 min.

Theoretical

Burner Model Equations. The description of the burner behavior is achieved by means of equations for mass continuity, gas-phase species conservation, separate gas-phase and porous medium energy conservation, and the ideal gas law. The model equations are solved in a one-dimensional domain for the space variable and in a time-dependent regime. The model accounts for longitudinal mass transfer phenomena in the gas phase, interphase heat transfer, internal radiation in the porous medium, and a detailed reaction mechanism (Kazakov and Frenklach, 2002) for methane combustion consisting of 104 reactions among 22 chemical species. The simulation software was interfaced with the Chemkin libraries (Kee et al., 1999a), so as to account for complex reaction mechanisms and for the calculation of all thermodynamic properties present in the model equations. Moreover, the Transport module (Kee et al., 1986) of the Chemkin package was used in the calculation of the transport properties of the gas mixture.

Continuity equation

$$\dot{m} = S\rho u \quad \text{(gas-only region)} \tag{1}$$

$$\dot{m} = S\varepsilon\rho u \quad \text{(gas–solid region)} \tag{2}$$

Mass balance

$$S\varepsilon\rho_g \frac{\partial Y_k}{\partial t} + \dot{m}\frac{\partial Y_k}{\partial z} + \frac{\partial (V_k S\varepsilon\rho_g Y_k)}{\partial z} - \bar{R}_k M_k S\varepsilon = 0 \qquad (k = 1, \ldots, K) \tag{3}$$

Gas phase energy balance

$$S\varepsilon\hat{c}_{pg}\rho_g \frac{\partial T_g}{\partial t} + \dot{m}\hat{c}_{pg}\frac{\partial T_g}{\partial z} + \sum_{\text{species},k} V_k Y_k S\rho\varepsilon\hat{c}_{pg,k}\frac{\partial T_g}{\partial z} + \frac{\partial}{\partial z}\left(-k_g S\varepsilon\frac{\partial T_g}{\partial z}\right) - \sum_{\text{species},k}\bar{R}_k M_k \hat{H}_k S\varepsilon + hS(T_g - T_S)a = 0 \tag{4}$$

Solid phase energy balance

$$S(1-\varepsilon)\hat{c}_{ps}\rho_s\frac{\partial T_s}{\partial t} + \frac{\partial}{\partial z}\left(-k_{s,\text{eff}}S\frac{\partial T_s}{\partial z}\right) - hS(T_g - T_s)a = 0 \tag{5}$$

Equation of state

$$\rho_g = \frac{p\bar{M}}{RT_g} \tag{6}$$

The diffusion velocity was calculated, according to the criteria suggested by Kee et al. (1999b), with a mixture-averaged formulation

$$V_k = v_k + w_k + C. \tag{7}$$

The first term on the right-hand side of Eq. (7) is the ordinary diffusion velocity and it is calculated by the Curtiss–Hirschfelder approximation (Curtiss and Hirschfelder, 1949) in terms of molar fraction gradients

$$v_k = -D_k\frac{1}{X_k}\frac{dX_k}{dz}. \tag{8}$$

The D_k coefficient is calculated by means of the transport package.

The second term is the thermal diffusion velocity (Chapman and Cowling, 1970)

$$w_k = -\frac{D_k\Theta_k}{T_g X_k}\frac{dT_g}{dz} \tag{9}$$

The last term, recommended by Coffee and Heimerl (1981), is the correction velocity C and emerges from the evidence that the sum of the diffusion velocities of all species must be zero

$$\sum_{\text{species},k} Y_k V_k = 0. \tag{10}$$

More details on the calculations of the diffusion velocity can be found in the article by Kee et al. (1999b).

The convection heat transfer coefficient was calculated on the basis of measurements reported by Golombok et al. (1991)

$$\text{Nu} = 0.04\,\text{Re}^{0.53} \quad (\text{Re} < 0.4) \tag{11}$$

$$\text{Nu} = 0.10\,\text{Re}^{1.64} \quad (\text{Re} > 0.4). \tag{12}$$

In the above correlations, both the Nusselt and the Reynolds numbers are based on the fiber diameter

$$\mathrm{Nu} = \frac{h' d_\mathrm{f}}{k_\mathrm{g}} \tag{13}$$

$$\mathrm{Re} = \frac{\dot{m} d_\mathrm{f}}{S \mu_\mathrm{g}}. \tag{14}$$

To shift from the area-based heat transfer coefficient to the volumetric one, the following equation is employed (Golombok et al., 1991)

$$h = \frac{4\ \mathrm{Nu}\ k_\mathrm{g}(1-\varepsilon)}{d_\mathrm{f}^2}. \tag{15}$$

The effective thermal conductivity accounts for both thermal conduction and radiation in the fiber matrix and was calculated according to the law proposed by Golombok et al. (1991) for metal fiber burners

$$k_{\mathrm{s,eff}} = \frac{k_{\mathrm{s,bulk}}(T)}{73} + 2.5 \cdot 10^{-11} T^3. \tag{16}$$

The first term of Eq. 16 accounts for thermal conduction. The bulk thermal conductivity is expressed in this law as a function of the solid-phase temperature. Due to the considerable temperature difference occurring between the inlet and outlet surfaces, the $k_{\mathrm{s,bulk}}$ term varies remarkably within the solid-phase domain. The empirical correlation used therefore

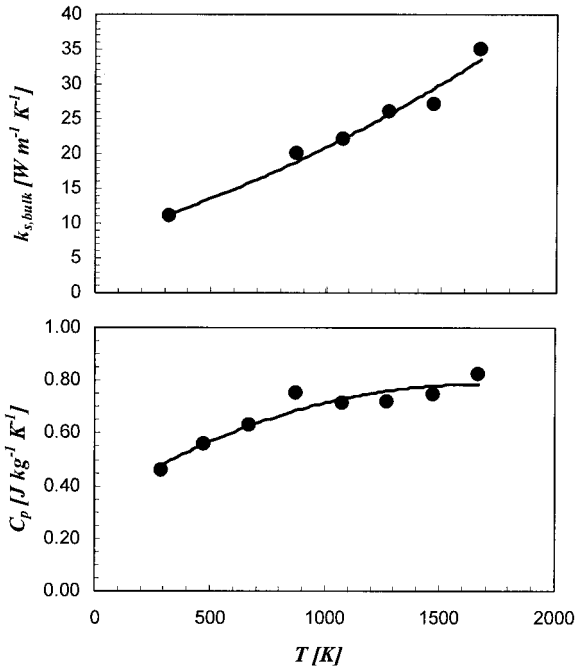

Figure 2. Experimental values of bulk thermal conductivity and solid-phase specific heat and the related fitting trend lines implemented in the model (courtesy of Kanthal, Sweden).

Table 1. Some Typical Values of the Burner Physical Parameters and Operating Conditions Used in This Study

Q	250–600 kW/m^2
E_a	5–35%
P	1 atm
S	0.04 m^2
L	2×10^{-3} m
d_f	5×10^{-5} m
e	0.8
ε	0.8
h	1.5×10^6–4×10^6 W m^3 K

was developed on the basis of experimental measurements of bulk thermal conductivity performed by the metal fiber producer (Kanthal, Sweden) as reported in Figure 2. In the same diagram, the heat capacity is reported as a function of the solid-phase temperature. The experimental values of $k_{\mathrm{s,bulk}}$ and $\hat{c}_{\mathrm{p,s}}$ were then fitted using polynomial equations ($R^2 = 0.98$ and 0.92, respectively). The porous medium exhibits a lower thermal conductivity in comparison to the solid bulk value, due to the lack of continuity in the fiber matrix. The reduction factor (1/73) is substantially in agreement with the value (1/80) that can be determined by the correlation reported by Mantle and Chang (1991) and also employed by Rumminger (1996). The second term of Eq. 16 accounts for radiation within the metal fiber matrix. Finally, the values of the other important physical parameters of the metal fiber burner are summarized in Table 1.

Appropriate boundary conditions are used, consisting of fixed values imposed at the domain inlet and of flat profiles at the outlet for the mass fractions and the gas phase temperature

$$Y_k|_{z=0} = Y_{k,\mathrm{feed}} \quad k = 1, \ldots, K \tag{17}$$

$$\left.\frac{dY_k}{dz}\right|_{z=L} = 0 \quad k = 1, \ldots, K \tag{18}$$

$$T_g|_{z=0} = T_{\mathrm{g,feed}} \tag{19}$$

$$\left.\frac{dT_\mathrm{g}}{dz}\right|_{z=L} = 0 \tag{20}$$

For the solid-phase temperature, a condition of energy conservation at the upstream boundary is imposed. In the following equation, the net energy output at the solid-phase boundary (right-hand side) due to radiation toward the surroundings and to convection between the impinging gas and the upstream surface is set equal to the energy flux in the solid by conduction and radiation (left-hand side) that reaches the surface

$$-k_{\mathrm{s,eff}} \left.\frac{dT_\mathrm{s}}{dz}\right|_{z=z_\mathrm{in}} = (\sigma e (T_\mathrm{s}^4 - T_\mathrm{room}^4) + h'_{\mathrm{surf}}(T_\mathrm{s} - T_\mathrm{g}))|_{z=z_\mathrm{in}}. \tag{21}$$

A modification of the equation reported by Kanury (1988) was employed for the calculation of the upstream convective heat transfer coefficient

$$\mathrm{Nu} = (1-\varepsilon) 0.57\ \mathrm{Re}^{0.5} \mathrm{Pr}^{0.4}. \tag{22}$$

The correlation was developed for a gas impinging onto a flat plate, but the term (1-ε) helps in taking into account the reduction of exchange area due to the void matrix structure. This approach was suggested and successfully employed by Rumminger (1996) to account for the heat exchange between the solid and the gas phase upstream of the porous medium.

At the downstream surface, the solid-phase temperature is calculated so as to satisfy an overall energy balance (Rumminger, 1996; Bouma, 1997)

$$\dot{m}\hat{c}_p(T_{ad} - T_g)\big|_{z=z_{exh}} = S\sigma e(T_s^4 - T_{room}^4)\big|_{z=z_{in}} + S\sigma e(T_s^4 - T_{room}^4)\big|_{z=z_{out}}. \quad (23)$$

The equation states that the total radiant loss from the burner (righthand side) equals the net convective heat transfer from the gas to the porous medium (lefthand side). The interphase heat transfer determines an exhaust gas temperature that is lower than the adiabatic value, and hence the net convective energy transfer was determined by employing an overall energy balance on the gas phase. The use of Eq. 23 at the downstream boundary instead of a correlation similar to Eq. 21 is strongly recommended in the literature (Rumminger, 1996; Bouma, 1997). The high temperature at the hot exit surface considerably increases the uncertainty on the heat transfer coefficients to be used in a correlation like Eq. 21, and therefore the use of an overall energy balance in this boundary condition can be considered more suitable.

The numerical method employed for the solution of the set of conservation equations consisted of the discretization of the space derivatives by means of an upwind finite-differences approach, according to the method of lines. The set of ordinary differential equations thus arising is large and stiff and therefore it required the selection of an appropriate integrator. The problem was solved by means of a robust initial value solver suitable for sparse systems of equations (Hindmarsh, 1983), implementing several numerical methods. The one employed in the solution of our model is a method based on backward differentiation formulas, a modification of Gear's method, with a numerically generated Jacobian matrix.

Analysis of the Burner Stability. The analysis of the burner stability and flashback was carried out according to the following procedure. The simulation was performed at specific values of the excess of air (E_a) and the specific power input (Q), until a steady-state solution was determined. The inlet gas temperature was initially set to 300 K (T_{room}). The inlet gas temperature was then progressively increased stepwise and the corresponding new steady-state solutions were determined by a continuation procedure, which started from the previously calculated solution. In this analysis, the dependence of the upstream burner surface temperature on the inlet gas temperature was calculated, and $T_{s,in}$ vs. $T_{g,feed}$ patterns were drawn. However, the feedstock preheating, and therefore the inlet gas temperature, is related to the upstream surface temperature. An energy conservation equation can be written by considering that the radiant flux in the backward direction determines the preheating of the feedstock

$$\dot{m}\hat{c}_p(T_{g,feed} - T_{room}) = S\sigma e(T_{s,in}^4 - T_{room}^4). \quad (24)$$

The equilibrium solutions of the system were obtained by coupling this equation with the $T_{s,in}$ vs. $T_{g,feed}$ pattern. The inlet gas temperature and the upstream surface temperature, in fact, should evolve toward such values that both Eq. 24 and the $T_{s,in}$ vs. $T_{g,feed}$ pattern, derived by the solution of the burner model Eqs. (1–23) via the continuation procedure, are satisfied.

Results and Discussion

Model validation

The comparison between measured and calculated burner surface temperatures is presented in Figure 3. The downstream surface temperature increases with the specific power input up to a maximum value: in this Q interval higher temperatures help to radiate the increasing energy input received by the porous medium from the solid phase. However, at higher specific power inputs (that is, higher mass-flow rates) the flame front moves downstream and therefore part of the energy that could be exchanged with the porous medium actually remains mostly confined in the gas phase, due to the progressive reduction of the contact time between gas and solid. If a further increase in mass flow rate were imposed, a partial flame lift off and burner cooling would occur. The trends in the surface temperatures can be further explained with the help of Figure 4, which shows the calculated temperature and methane concentration profiles in the burner at two different specific power inputs. The burner exhibits two distinct regions: at the porous medium entrance the solid preheats the gas (zone I) that, as the temperature rises, is ignited and releases the energy of methane combustion. As this occurs, the gas temperature overcomes that of the solid and the interphase heat flux is inverted, that is, the solid receives energy from the gas phase (zone II). An increase in the specific power input (from Figure 4a to 4b) forces the concentration profiles to move downstream as the result of a higher mass flow rate of the feed gas mixture. Furthermore, concentration profiles become steeper, because, when the reaction starts, a higher energy release from the gas phase takes place as a consequence of the increased methane input in the system. This determines a raise in the downstream surface temperature, which further promotes faster reaction kinetics. The reaction zone inside the porous medium therefore gets reduced and moves toward the downstream burner surface. The region of gas preheating (zone I) is expanded, that is, the location of the "equilibrium" temperature (where the solid and the gas phase have the same temperature) moves downstream, whereas the upstream surface temperature becomes lower. These considerations hold as far as the reaction is occurring, at least in part, within the porous medium (that is, in the radiant operating mode for the burner). When the feed flow rate further increases, methane conversion within the porous medium becomes marginal and transition to the blue flame mode takes place.

In the context of the present study, the above described capability of reproducing the physics of the system in terms of thermal behavior and of axial temperature profiles represents one of the most important features of the model. This is necessary for the understanding of flashback. The mass-flow rate and the methane concentration in the feedstock (Q and E_a) determine in fact the position of the equilibrium point, which affects in turn the upstream surface temperature. This plays a

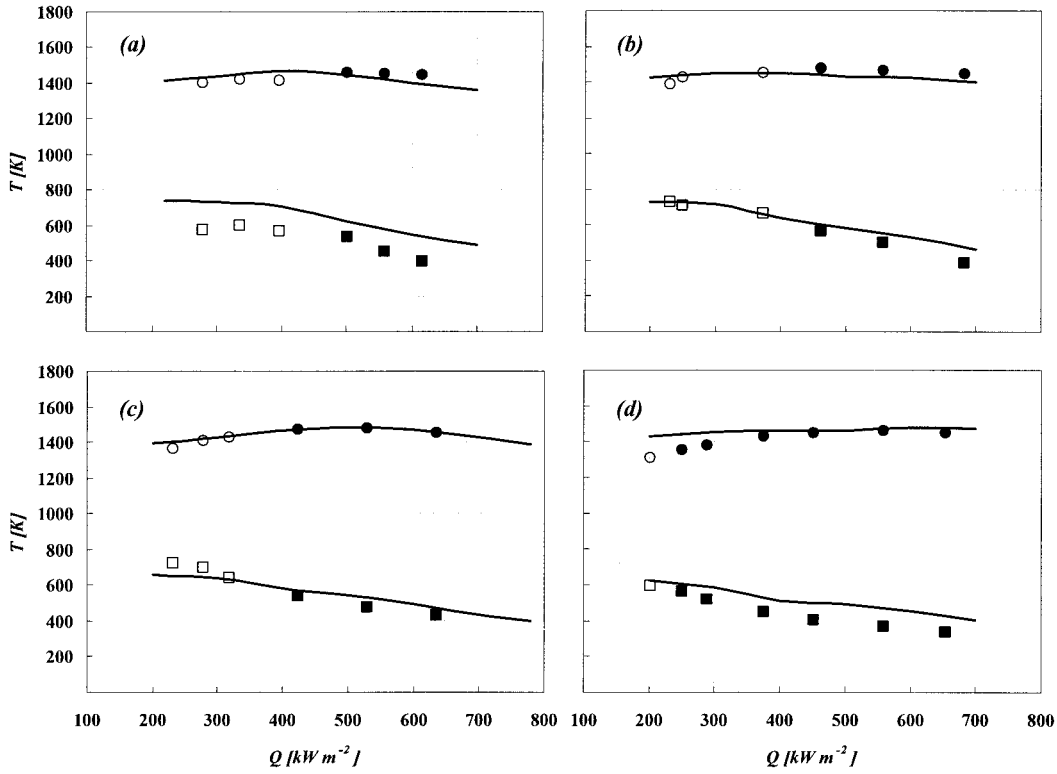

Figure 3. Experimental upstream (circles) and downstream (squares) surface temperatures compared with model calculations (lines, Eqs. 1–23).

Excess of air values: (a) E_a = 5%; (b) E_a = 10%; (c) E_a = 15%; (d) E_a = 30%. Empty markers: flashback occurred within 15 min; data collected after 1 min. Filled markers: no flashback observed.

major role in determining the flashback, as will be discussed in the next paragraph.

Figure 5 represents the carbon monoxide/dioxide emissions of the burner. It can be seen that the model can reproduce quite satisfactorily the trend of CO emissions at high power inputs, but fails at low Q, probably due to effects of cooling exerted by the burner sealed perimeter. A two-dimensional (2-D) model would be necessary to account for this effect, which is, however, not critical for flashback prediction.

Flashback analysis

As a preliminary analysis, the influence of the feedstock preheating on methane concentration and solid-phase temperature profiles is shown in Figure 6. As the inlet temperature increases, the methane concentration profile moves upstream and the burner temperatures rises as a result of the enhanced gas-phase reactivity due to feedstock preheating. Once $T_{g,feed}$ reaches a sufficiently high value, $X_{CH4,in}$ at the burner upstream surface steeply drops, since the flame front moves ahead of the porous medium (flashback).

The calculation methodology here presented was conceived in order to reproduce the physics of the flashback phenomena occurrence. Immediately after the burner startup, the plenum chamber housing is still relatively cold and the combustion therefore takes place only inside the porous medium. As the combustion starts inside the metal fiber mat, the temperature of the upstream surface of the porous medium becomes relatively high reaching, for example, one of the values indicated in

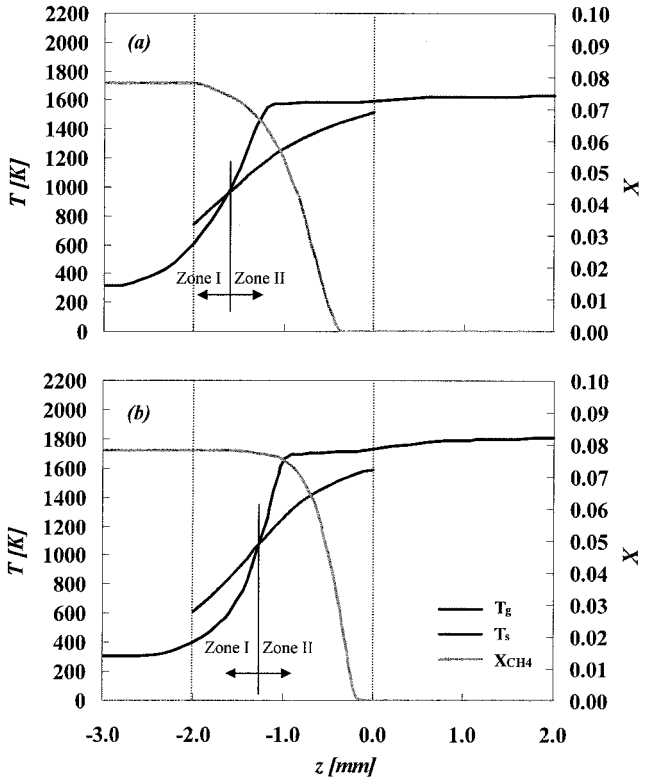

Figure 4. Methane concentration and thermal profiles along the burner axial coordinate (E_a = 15%): (a) Q = 220 kW/m^2; (b) Q = 550 kW/m^2.

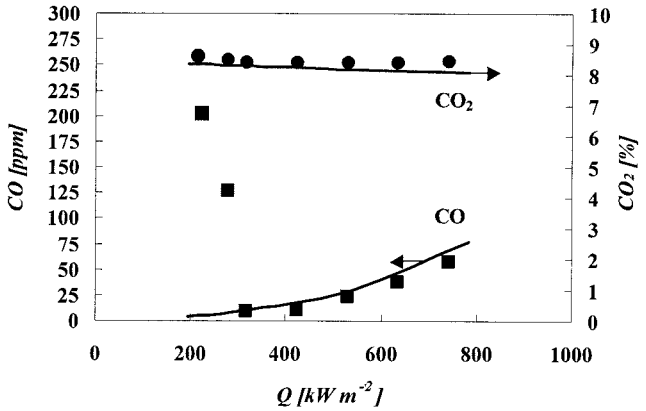

Figure 5. Comparison between calculations and experimental values of CO and CO_2 emissions (E_a = 15%).

Figure 3. These conditions occur with a feedstock inlet temperature of 300 K. However, the upstream surface temperature induces a backward-directed radiant energy flux, as stated by the boundary condition Eq. 21. This radiant flux can be received by the burner housing, thus preheating the feedstock, which in turn determines a further move of the flame front inside the porous medium and a further enhancement of the upstream surface temperature as well as of the preheating effects.

The calculation approach adopted in this work decouples these recurring phenomena and analyzes them separately. One of the objectives of the present analysis is to point out that the proposed physical mechanism based on the backward-directed radiant energy flux allows one to explain the available experimental data.

At first, the dependence of the upstream surface temperature with the amount of feedstock preheating is assessed. As mentioned, therefore, the dependence of the model solution on the inlet gas temperature $T_{g,feed}$ at fixed values of E_a and Q has been performed by means of a continuation procedure. The upstream surface temperature of the porous medium, obtained by model calculations (Eqs. 1–23), was plotted versus $T_{g,feed}$ in Figure 7 at fixed values of Q and E_a. When the sigmoid-shape curve is observed, the surface temperature rises with $T_{g,feed}$ and when flashback occurs a steep increase takes place.

As a second step, the pre-heating is related to the upstream surface temperature. As a consequence, the parabolic-shape curve related to Eq. 24 is plotted on the same diagram of Figure 7. Obviously, equilibrium is reached when both conditions are satisfied.

Steady-state multiplicity can be seen. The intersections of mentioned curves give the possible asymptotic solutions of the physical system, and typically three points can be singled out. The solution marked "A" in Figure 7 represents the stable solution that takes place in a normal burner operation: the flame front is located at least in part within the porous medium, $X_{CH4,in}$ is nearly at the feedstock value and the upstream surface temperature is remarkably lower than 1000 K. At higher temperatures (point "C") a flashback solution is possible as the flame front gets stabilized ahead of the porous medium (see the high upstream surface temperature). Finally, there is an unstable solution: the intermediate point "B." The system is attracted by the stable solutions A and C moving either on the left or on the right side of B, respectively.

The approach resulting in Figure 7 has been repeated many times at different values of Q and E_a, and this allowed the calculation of the hysteresis cycles represented in Figure 8. In particular, each hysteresis curve was obtained at a fixed E_a value by changing the specific power input Q from high values (lower branch of the curve) to low values (flashback region). As the system operates under stable conditions on the low-temperature branch of the hysteresis curve, the burner operation remains stable without flashback. The flame front is stabilized within the porous medium and the upstream surface temperature is relatively low. As the gas inlet temperature is increased, the system goes across a region of multiple steady states, until the high-temperature branch of the curve is reached. Under these conditions, the flame front stabilizes ahead of the porous medium and the surface temperature steeply increases. It is therefore possible to single out different regions where flashback certainly occurs, where it might take place depending on the starting burner conditions (transition), and where flashback is impossible.

The same results can be represented more conveniently on the E_a–Q plane (Figure 9), which points out the safe operation region and the flashback region.

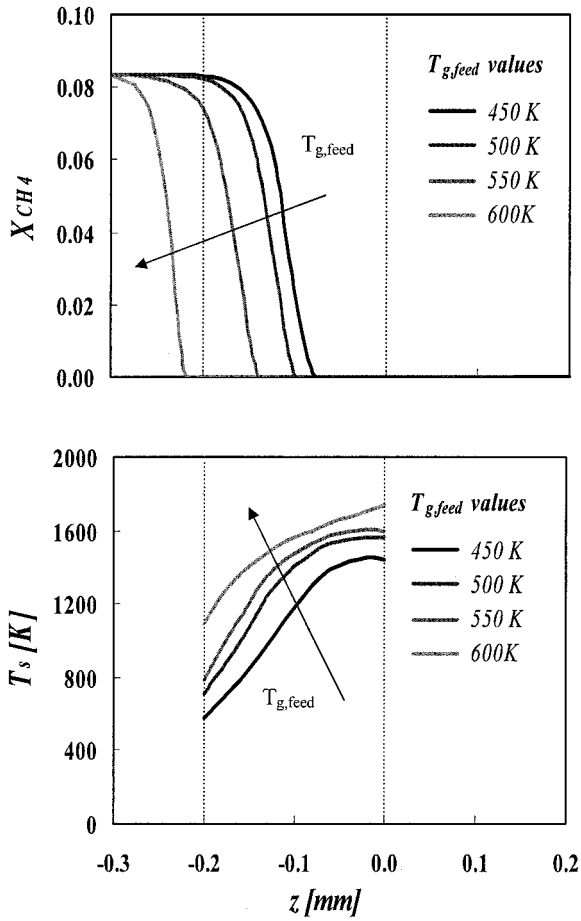

Figure 6. Calculated methane molar fraction profiles (a) and solid-phase temperature profiles (b) at Q = 700 kW/m^2 and E_a = 15%, at different values of inlet gas temperature.

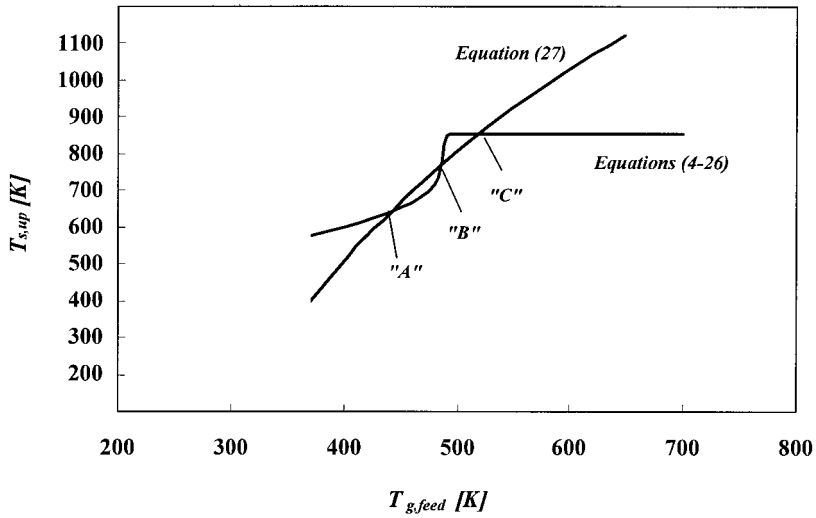

Figure 7. Upstream surface temperature versus inlet gas temperature.

The intersections between the curves represent the steady-state solutions of the burner. $Q = 500$ kW/m^2; $E_a = 15\%$.

At higher Q values, the flame front naturally shifts downstream at otherwise constant conditions, hence improving the resistance of the system toward flashback. Similar considerations hold if one considers the dependence of the system behavior on the excess of air. A lean mixture (higher E_a values) forces the concentration profiles to move downstream, because the same power input can only be achieved by a higher total mass-flow rate. This determines an increase in the system stability and higher $T_{g,feed}$ are required to make flashback occur. Therefore, the system exhibits a more critical behavior in the region of low specific power inputs and low excess of air as the radiant heat mode is promoted.

In Figure 9 experimental data points concerning the stable operating conditions registered at the lowest possible Q value among those investigated for each excess air value (Figure 3) are reported. Model predictions concerning the borderline of flashback occurrence region are in rather good agreement with such data points, which strengthens the arguments proposed in the next section concerning the amelioration of the burner control system.

It can be finally pointed out that the fair agreement between calculations and experiments supports the interpretation of the flashback occurrence based on the proposed mechanism of the backward-directed radiant energy flux.

Flashback avoidance: control issues

The current trend in burner technology for domestic applications is to obtain, within a single heating unit, hot water for domestic use as well as for household heating. For an average

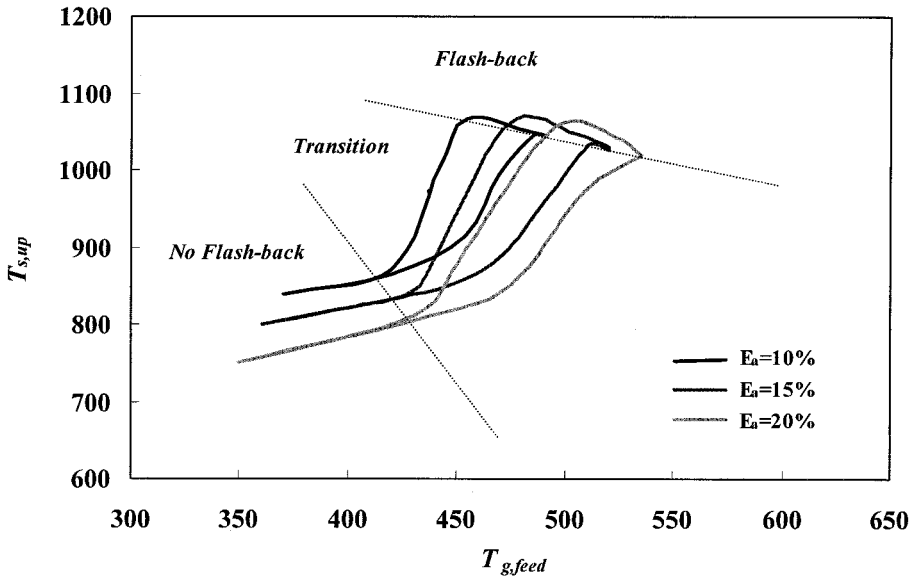

Figure 8. Ignition and light-off cycles: hysteresis curves and flashback regions in the $T_{g,feed}$ vs $T_{s,in}$ plane obtained when varying Q for different E_a values.

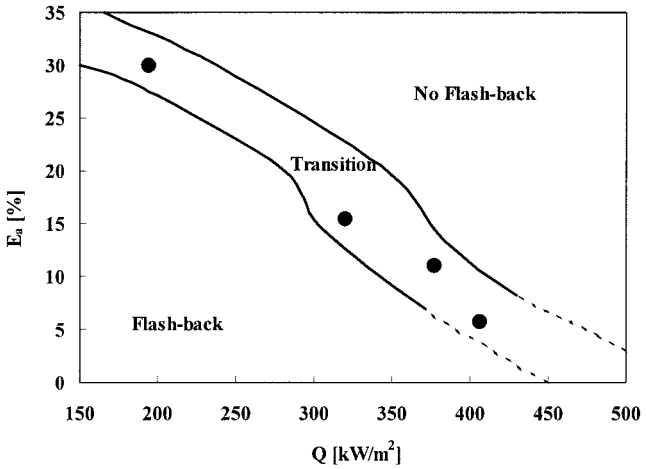

Figure 9. Flashback charts in the E_a–Q plane. The filled symbols represent the highest Q value experimentally observed at which flashback takes place within 15 min (see Figure 3).

family house some 25 kW are needed for any occasional sanitary purposes (showers, hot water for cooking, and so on) whereas just 2–3 kW are steadily required for ambient air temperature conditioning. This entails that the burner must be operated continuously and should possess a very wide heat modulation range (10:1 turndown ratio), unless high hot water storage and the consequent heat dissipation are accepted.

Most of this high modulation range should be confined in the radiant heat mode, so as to maximize heat exchange effectiveness and boiler efficiency. This forces the minimum of the modulation range to be set at the lowest possible Q values for ambient air heating. The blue flame mode should be limited to the peaks in the energy demand corresponding to hot sanitary water production.

The main purpose of this study was to figure out an optimal strategy for burner control, aimed at improving the amplitude of the power modulation range, with no occurrence of flashback.

The conventional burner modulation system is depicted in Figure 10a. Any variation in the power requirement is obtained by a change in the rotational speed of the air feed fan. As a consequence of the modified air flow the pressure drop across the burner system is changed. This is noted by a pressure indicator, which through a pneumatic system modifies proportionally the flow rate of natural gas delivered through a valve. By these means the excess air value can be kept constant over the entire modulation range rather cheaply. Air and methane get mixed within a Venturi-type mixer, selected for its low pressure drop. Figure 11 shows how the selected excess air generally lies in the range between 15 and 20%. E_a values falling below 15% entail some risk of unacceptable CO and unburned HC emissions, whereas higher excess air ratios than 20% are avoided as boiler efficiency gets lower when E_a increases.

However, when Q is decreased at constant E_a, the flashback conditions are approached rather quickly and a lower limit to burner power modulation can be clearly identified when the conventional control strategy line crosses the flashback region borderline (Figure 11).

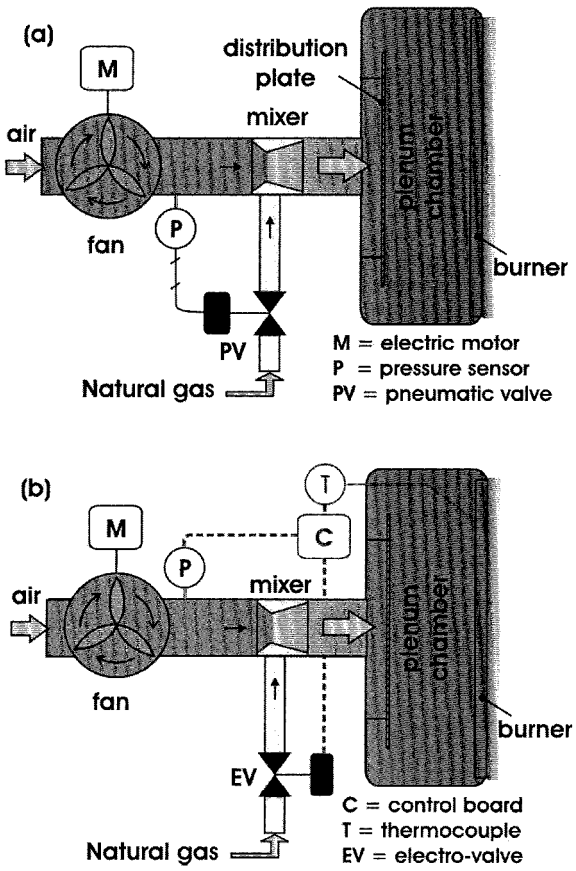

Figure 10. Conventional (a) and advanced (b) control strategies outlined over the E_a–Q flashback chart.

According to the considerations proposed so far, the resistance to flashback gets worse as the upstream burner temperature increases, with all other conditions being constant. An advanced control system based on the direct measurement of $T_{s,in}$ is being examined. The focus of our stability analysis was on the upstream surface temperature strictly because this measurable variable can be practically employed in the implementation of the burner control strategy (Figure 10b). A thermocouple could in fact be placed in the plenum chamber, choosing

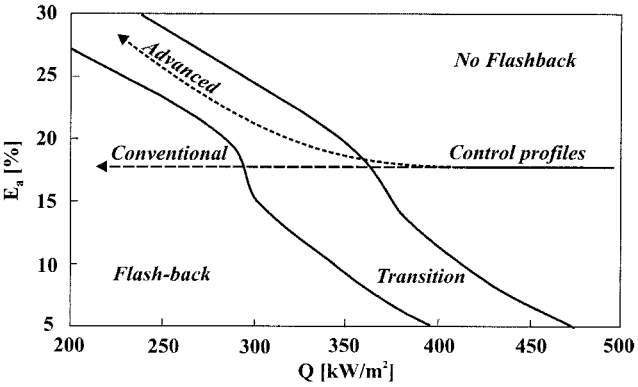

Figure 11. Conventional (a) and advanced (b) control systems.

its position so as to maximize the sensitivity of the system control. A possible appropriate position for the thermocouple could be near the upstream burner surface. As the thermocouple reveals a temperature increase over a threshold value for safe operation, indicating the approach of a flashback phenomenon, the control system could manipulate the excess of air by a suitable modification of the methane flow rate via an electrical valve, according to the prescriptions of ad hoc developed control board. Such a control board should obviously take into account the output of the burner pressure-drop indicator as well. Since the reduced methane flow rate determines a reduction of both the inlet methane mass fraction and the total flow rate, this control strategy reduces E_a and, simultaneously, Q. The advanced control strategy drawn in Figure 11 can be thus followed. This line is selected on the grounds of the following criteria:

Get to lower minimum Q values than those allowed by the conventional control system for the sake of maximizing operation in the radiant regime;

Keep the excess air values as low as possible not to suffer too much from loss of boiler efficiency; and

Keep costs as low as possible.

Conclusions

A mathematical model of a premixed radiant burner was presented and its performance was validated against experimental data produced in our laboratories. The model reproduces the typical thermal behavior of metal fiber burners observed in the whole range of excess of air and specific power input investigated. The upstream and downstream porous medium surface temperatures in particular are satisfactorily predicted, and the typical trends of these variables were enlightened in terms of feedstock mass-flow rate and methane composition (Q and E_a). The success in determining the thermal behavior of the burner is of crucial importance in understanding flashback resistance, which is eventually related to the upstream surface temperature. Model calculations and experiments were compared also for the CO and CO_2 emissions, showing that the model can reproduce the measured values, except at very low Q values. This could be ascribed to two-dimensional effects, related to the gas cooling exerted at the burner sealing perimeter, which is considered responsible for high CO emissions.

A model criterion for the analysis of stability and flashback of a metal fiber burner was thus formulated. The "mechanism" of flashback behavior is based on the occurrence of backward-directed radiant energy flux that preheats the feedstock. This in turn determines an increase in the gas phase reactivity and thus a shift of the methane concentration profile further inside the porous medium. As a consequence, the upstream surface temperature and that of the backward-directed radiant energy flux increase.

Based on the proposed analysis methodology, it was possible to determine regions where multiple steady states are possible. In particular, a range of conditions of safe operation and a flashback region could be singled out in an E_a-Q chart. Model predictions of flashback occurrence are in fair agreement with experimental observations, thus supporting the proposed flashback mechanism based on the backward-directed radiant energy flux.

The results described above allowed one to propose an advanced burner control system for the purpose of avoiding flashback over an as-wide-as-possible power modulation range within the radiating regime. Some guidelines for an optimal control strategy were presented and a new technical solution for the control system based on a thermocouple measurement just upstream the burner surface. Studies are in progress to implement this strategy within a power-modulating commercial boiler.

Acknowledgments

The financial support of the European Community is gratefully acknowledged (Energy Project HIMOCAT: "High-modulation, high-efficiency and low-emission boilers for household application based on premixed catalytic burners").

Notation

a = gas-solid interphase area, m^{-1}
$\hat{c}_p$ = specific heat, J $kg^{-1}K^{-1}$
C = correction velocity, m s^{-1}
d = diameter, m
D = diffusivity, m^2s^{-1}
e = solid phase emissivity
E_a = excess of air, %
$\Delta\hat{H}$ = reaction enthalpy, J kg^{-1}
$\hat{H}$ = enthalpy of a chemical species, J kg^{-1}
h = volumetric heat transfer coefficient, J K^{-1} $m^{-3}s^{-1}$
h' = area-based heat transfer coefficient, J K^{-1} $m^{-3}s^{-1}$
J_E = energy flux, J s^{-1}
k = thermal conductivity, J s^{-1} m^{-1} K^{-1}
K = total number of chemical species involved in the reaction environment
L = solid phase domain length, m
$\dot{m}$ = gas phase mass flow rate, kg s^{-1}
$\underline{M}$ = molar weight, kg mol^{-1}
$\overline{M}$ = mean molar weight, kg mol^{-1}
Nu = Nusselt number
P = pressure, atm
Q = specific power input, kW m^{-2}
$\underline{R}$ = universal gas constant, J K^{-1} mol^{-1}
$\overline{R}$ = chemical production rate of a species, mol $m^{-3}s^{-1}$
Re = Reynolds number
S = reactor cross-flow section, m^2
t = time variable, s
T = temperature, K
u = gas phase velocity, m s^{-1}
v = ordinary diffusion velocity, m s^{-1}
V = diffusion velocity, m s^{-1}
w = thermal diffusion velocity, m s^{-1}
X = mole fraction
Y = mass fraction
z = space variable, m

Greek letters

ε = porosity
μ = gas viscosity, kg $m^{-1}x^{-1}$
ρ = gas phase density, kg m^{-3}
σ = Stefan–Boltzman constant, J s^{-1} m^{-2} K^{-4}
θ = thermal diffusion ratio

Subscripts

ad = adiabatic
bulk = bulk
comb = combustion
eff = effective
exh = exhaust gas

f = fibre
$feed$ = feedstock gas
g = gas phase
k = generic species
in = solid phase inlet (upstream surface)
out = solid phase outlet (downstream surface)
ov = overall
$room$ = ambient conditions
s = solid phase
$surf$ = surface
tip = thermocouple tip

Literature Cited

Bird, R. B., W. E. Stewart, and E. N. Lightfoot, *Transport Phenomena,* Wiley, New York (1960).

Bouma, P. H., *Methane–Air Combustion on Ceramic Foam Surface Burners*, Ph.D.thesis, Eindhoven University of Technology (1997).

Bouma, P. H., private communication (2000).

Cerri, I., G. Saracco, V. Specchia, and D. Trimis, "Improved Performance Knitted Fibre Mats as Supports for Premixed Natural Gas Catalytic Combustion," *Chem. Eng. J.* **82,** 72 (2001).

Chapman, S., and T. G. Cowling, *The Mathematical Theory of Non-Uniform Gases*, Cambridge University Press, Cambridge (1970).

Coffee, T. P., and J. M. Heimerl, "Transport Algorithms for Premixed Laminar, Steady-State Flames," *Combust. Flame* **43,** 273 (1981).

Curtiss, C. F., and J. O. Hirschfelder, "Transport Properties of Multicomponent Gas Mixtures," *J. Chem. Phys*. **17,** 550 (1949).

Golombok, M., A. Prothero, L. C. Shirvill, and L. M. Small, "Gas Temperature Above a Porous Radiant Burner: Comparison of Measurements and Model Predictions," *Combust. Sci. Technol.* **77,** 233 (1991).

Hargreaves, K. J. A., H. R. N. Jones, and D. B. Smith, "Developments in Burner Technology and Combustion Science," Proc. of the Institution of Gas Engineers Autumn Meeting, Paper No. 1309, p. 31, London (1986).

Hindmarsh, A. C., "Odepack, a Systematized Collection of Ode Solvers," in *Scientific Computing*, R. S. Stepleman et al., eds., North-Holland, Amsterdam, p. 55 (1983).

Kanury, A. M., *Introduction to Combustion Phenomena*, 5th ed., Gordon and Breach, New York (1988).

Kazakov, A., and M. Frenklach, "Reduced Reaction Sets Based on GRI-Mech," University of California at Berkeley, available at http://www.me.berkeley.edu/drm (2002).

Kee, R. J., G. Dixon-Lewis, J. Warnatz, M. E. Coltrin, and J. A. Miller, "A Fortran Computer Package for the evaluation of Gas-Phase, Multicomponent Transport Properties," Sandia National Laboratory Report No. SAND86–8246 (1986).

Kee, R. J., F. M. Rupley, J. A. Miller, M. E. Coltrin, J. F. Grcar, E. Meeks, H. K. Moffat, A. E. Lutz, G. Dixon-Lewis, M. D. Smooke, J. Warnatz, G. H. Evans, R. S. Larson, R. E. Mitchell, L. R. Petzold, W. C. Reynolds, M. Caracotsios, W. E. Stewart, and P. Glarborg, *CHEMKIN Collection*, Release 3.5, Reaction Design, San Diego, CA (1999a).

Kee, R. J., F. M. Rupley, J. A. Miller, M. E. Coltrin, J. F. Grcar, E. Meeks, H. K. Moffat, A. E. Lutz, G. Dixon-Lewis, M. D. Smooke, J. Warnatz, G. H. Evans, R. S. Larson, R. E. Mitchell, L. R. Petzold, W. C. Reynolds, M. Caracotsios, W. E. Stewart, and P. Glarborg, *Premix User Manual,*, CHEMKIN Collection 3.5, Reaction Design, San Diego, CA (1999b).

Mantle, W. J., and W. S. Chang, "Effective thermal conductivity of sintered metal fibres," *J. Thermo-phys. Heat Transf.* **5,** 545 (1991).

Rumminger, M. D., "Numerical and Experimental Investigation of Heat Transfer and Pollutant Formation in Porous Direct-Fired Radiant Burners," PhD Diss., University of California at Berkeley, Berkeley, CA (1996)

Saracco, G., I. Cerri, V. Specchia, and R. Accornero, "Catalytic Premixed Fibre Burners," *Chem. Eng. Sci.* **54,** 3599 (1999).

Xiao, X., C. W. Choi, and I. K. Puri, "Measurements in Steady Two-Dimensional Partially Premixed Flames Using Laser Interferometric Holography," *Comb. Flame,* **120,** 318 (2000).

Manuscript received Aug. 31, 2003, and revision received Dec. 9, 2003.